Generalized Analysis Method for Magnetic Energy Harvesters

Daniel Monagle, *Graduate Student Member, IEEE*, Eric Ponce, and Steven B. Leeb, *Fellow, IEEE*

***Abstract*—Large-scale deployment of low-power sensing and computing units calls for unique power management solutions to overcome the inconvenience, costs, and waste problems associated with batteries. Energy harvesting offers an exciting solution to the battery problem, enabling circuits that can power themselves on-site from available ambient energy. Magnetic energy harvesters (MEHs), configured as current transformers, extract energy from the magnetic fields surrounding current-carrying power lines. As maximum power harvest occurs when a magnetic core is on the verge of saturation or saturated to some degree, modeling of magnetic energy harvesters is inherently difficult and nonlinear. This article proposes generalized analytical methods for modeling magnetic energy harvester behavior and validates these methods along with existing circuit model techniques. Intuition for core saturation behavior is presented and agreement with existing models is discussed. The analysis is motivated by addressing the feasibility of a split core magnetic energy harvester to power a microcontroller unit, and the models are experimentally validated for multiple harvester cores.**

***Index Terms*—Air gap, energy harvesting, inductor, magnetic, permeability, saturation, split core.**

I. Introduction

CONDITION-BASED maintenance (CBM) of electromechanical machines is essential for deploying automation in factories, transportation systems, and other mission-critical platforms. CBM systems continually monitor loads of interest in order to try to identify faults before they happen. Energy harvesting systems that eschew the use of batteries improve reliability and reduce maintenance requirements for sensor nodes for CBM systems.

Ambient energy harvesting is an attractive means of powering nonintrusive sensing systems for an extended period of time. Energy harvesting eliminates power wiring for wireless sensor networks, CBM, and Internet of Things devices. A "self-powered" system that harvests energy from some nearby source of energy (i.e., temperature differences, vibration, solar, wind, and magnetic fields) in the ambient environment allows for a one-time installation that requires little to no maintenance as it provides sensed data.

While common energy harvester sources, such as solar and airflow, may provide higher energy densities than magnetic field energy harvesting schemes [1], and motor control rooms and other industrial electromechanical housing areas often are exposed to little or no sunlight and airflow. Magnetic energy harvesting is an appealing choice for powering an electromechanical CBM unit, since typical primary or load current ranges for electromechanical loads might range from approximately 1–100-A rms at utility line frequencies. These load currents yield predictable power harvests from the associated magnetic fields at levels high enough for powering microcontroller units (MCUs) and sensing devices [2], [3]. Several works have explored the viability of MEHs as power sources for sensors and other monitoring units [4]–[9]. Bowtie [4] and helical [5] core geometries, however, are subject to a demagnetization phenomenon, which involve special manufacturing processes, and generally exhibit lower power densities than current transformer (CT) harvesters. An MEH installed on a current-carrying conductor successfully powered an MCU from the 10-kHz ripple current present in a kiloWatt motor drive, but this harvester was not configured as a CT, and a unique FEM modeling approach was used to optimize the design [6]. Vos [7], introduced complex permeance as a useful parameter for characterizing 50-/60-Hz CT MEHs, but magnetic saturation effects were not considered. Bhuiyan et al., [8] focused analytical modeling toward voltage capabilities of multilayer gapped cores made from flexible magnetic materials. Paul et al., [9] introduced the concept of a "dual-core" design, using concentric CT toroids of different magnetic materials, with the aim of avoiding saturation during harvester operation.

Several references have presented models for CT MEHs in both unsaturated and saturated regimes, including [10]–[12]. Core saturation modeling is of special interest because maximum power harvest occurs when the magnetic core is saturated [2], [11]. Zhou et al., [10] developed models for a resistive load on the CT harvester core, which is not representative of the more valuable use of an MEH, where the load is an approximately constant dc voltage, e.g., the supply rail of an MCU. Similarly, Zhuang et al. [12] presented an analytical modeling in terms of a "load index" dependent on the assumption of a resistive load. Park et al., [11] presented a core saturation model based on experimental measurements. Moon and Leeb [2], described magnetic energy harvester performance in both unsaturated and saturated operating regimes for an ungapped extremely high-permeability nanocrystalline toroidal core configured as a

Manuscript received 5 May 2022; revised 30 June 2022; accepted 23 July 2022. Date of publication 29 July 2022; date of current version 6 September 2022. This work was supported by the Office of Naval Research Structural Acoustics Program and the Grainger Foundation. Recommended for publication by Associate Editor J. Acero. *(Corresponding author: Daniel Monagle.)*

The authors are with the Department of Electrical Engineering and Computer Science, Massachusetts Institute of Technology, Cambridge, MA 02139 USA (e-mail: monagled@mit.edu; eaponce@mit.edu; sbleeb@MIT.EDU).

Color versions of one or more figures in this article are available at https://doi.org/10.1109/TPEL.2022.3195149.

Digital Object Identifier 10.1109/TPEL.2022.3195149

CT under both resistive and dc voltage load conditions. The analytical modeling in [2], however, relies on assumptions that can only be made for an extremely high-permeability core over a given range of primary current excitations. Also, ungapped toroidal MEHs configured as CTs require a break in the wiring for installation. This makes installation of the ungapped toroidal MEH intrusive.

A cut or split core enables simpler installation. The presence of cuts or gaps in the core, however, significantly affects the core power harvest capabilities. This article develops general models and design techniques for split core MEHs as a viable energy harvester solution for self-powered sensing and computing nodes. This article proposes a general model to describe MEH behavior over unsaturated and saturated operating regimes. Parallels between the existing model proposed in [2] and the generalized model are drawn, and an intuitive understanding of core saturation behavior is discussed. Both analytical and circuit modeling techniques are verified experimentally for a variety of nanocrystalline cores, and insight into harvester design optimization is provided.

The key contributions of this article are as follows. A generalized analytical model for power harvest predictions of a saturable CT magnetic energy harvester is proposed and experimentally verified. Unlike existing literature [2], [11], this model does not rely on the assumption that the magnetic core has an extremely high effective permeability. The analytic model presented as follows provides design insight and opportunity for optimization through numerical sweeps that a designer does not enjoy the capabilities of when only employing existing SPICE modeling techniques. The analytical modeling, in contrast to SPICE, highlights parameter relationships and tradeoffs, which can be exploited by a designer. Furthermore, such modeling can be used in real-time by a processing system compared to an intensive numerical solver, such as SPICE. The analysis in this work precisely quantifies both the opening time and closing time of a harvester "transfer window," the fraction of a half cycle of utility line current during which a saturable magnetic core delivers power to a load. This analysis allows us to probe practical definitions of saturation in the context of magnetic energy harvesters. Of the many possible definitions for magnetic saturation, we define the saturation boundary for CT magnetic energy harvesters based on the length of this "transfer window," and show analytically, in SPICE simulation, and experimentally the surprising and unintuitive result that maximum power harvest can occur when a magnetic core is saturated to some degree. Finally, output power levels over 30 mW are demonstrated using nanocrystalline split core CT magnetic energy harvesters, supporting the viablity of easily installed split core magnetic energy harvesters as power sources for low-power sensing and computing units.

II. Split Core Analysis

This section first describes existing circuit modeling techniques for CT MEHs. Next, generalized analytical techniques for modeling CT MEH saturation behavior and power output capabilities are proposed in detail. Finally, design intuition and agreement with existing models are discussed.

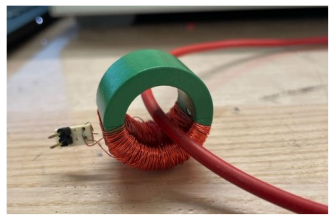

Fig. 1. Harvester prototype installed around primary wire.

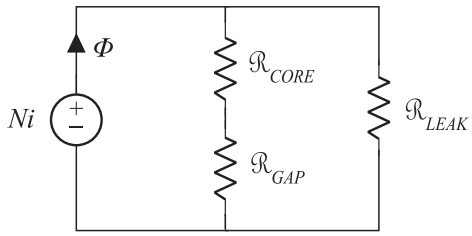

Fig. 2. Split core magnetic circuit model showing reluctance paths of magnetic material, gap, and leakage.

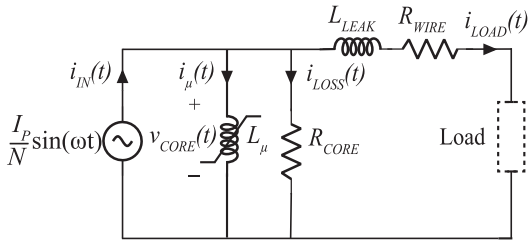

Fig. 3. Secondary-side split core MEH electric circuit model.

A. Circuit Modeling

Fig. 1 shows a prototype of our split core energy harvester.

The core consists of two semitoroids clamped around a single turn of the primary-side conductor, similar to the mechanical setup of a CT. A magnetic circuit model describing the split-core harvester is shown in Fig. 2, where the reluctances due to the two semitoroids of high-permeability nanocrystalline core material are lumped into a single-core reluctance, the reluctances due to the two air gaps are also lumped into a single-gap reluctance, and a single-lumped leakage reluctance is shown in parallel with the core path.

The corresponding secondary-side electric circuit model for our split-core harvester is shown in Fig. 3, where I_P refers to the CT harvester primary current, N refers to the number of secondary turns, L_μ is the saturable magnetizing inductance of the harvester core, R_{CORE} is a lumped resistance that models the core losses, L_{LEAK} is the leakage inductance of the harvester core, R_{WIRE} is the dc wire resistance of the core secondary winding, and ω is the primary current frequency in radians per second. By duality between magnetic and electric circuit models, parallel reluctances map to series inductances. L_{LEAK} is positioned in series with the load, as consistent with the

standard transformer model, including leakages [13]. The reflected primary-side leakage is made irrelevant by our choice of a current-source-driven transformer model.

For nanocrystalline cores in CBM applications, core loss is negligible in most cases. In CBM and other industrial electromechanical sensing applications, the MEH input current will likely operate at or around utility line frequencies, which are typically 50 or 60 Hz. Nanocrystalline alloys have been shown to demonstrate extremely low losses both at 60Hz [2] and even into the low 1–10-kHz range [14], [15]. The extremely thin hysteresis loop of nanocrystalline materials, along with their extremely low eddy current losses according to the IEM-5 parameter model [14], [15], account for the low overall core losses. For reference, the commercially available Vitroperm 500 F nanocrystalline magnetic material exhibits a core loss density less than 0.02 W/kg at a sinusoidal frequency of 50 Hz and saturation flux excitation of 0.9 T. The split cores used in this work are approximately 33 g, and assuming that they exhibit similar core losses to Vitroperm, would show less than 1 mW of loss at these utility line frequencies and flux excitation levels. Core loss is, therefore, ignored in this work. In other words, $i_{\text{LOSS}}(t) \approx 0$ is assumed for the analysis in this article. For extremely power-constrained designs or those where the magnetic material used has significantly higher losses, a method for calculating a non-negligible R_{CORE} is included in [2].

In many designs, such as those documented in this work, L_{LEAK} may be negligible, as verified through measurement, and R_{WIRE} will be relatively negligible compared to the effective load resistance. These parasitic components, therefore, are ignored in the analytical modeling section described later in this report. In some cases, particularly those where the harvester design warrants a very higher number of turns N, R_{WIRE} may not be negligible. In these cases, the value of R_{WIRE} can be reliably analytically predicted based on conductor material choice, wire gauge, and overall length, or R_{WIRE} can be measured using an impedance analyzer. The overall structure of our proposed analytical model still applies; however the designer should be aware that the harvester core voltage v_{CORE} will now see an additional voltage drop across the non-negligible R_{WIRE}. Therefore, the designer should not assume that the core voltage and load voltage are equal in the analysis, but rather that the core voltage is equal to load voltage plus the $i_{\text{LOAD}}(t) * R_{\text{WIRE}}$ additional voltage drop.

The air gap reluctance associated with our clamped split core harvester is a function of a relatively small air gap length on the order of the roughness of the mating surfaces of the semitoroids. Despite the significant difference in relative permeability of the core material and air gap, it is not accurate to conclude that the air gap reluctance dominates the total reluctance of the flux path. The relatively small air gap is simply a byproduct of cutting the core in order to meet the goal of easy noninvasive installation. The harvester is more precisely modeled, including both core material and air gap series reluctances. While these series reluctances could be modeled as parallel inductances in an equivalent electrical circuit, and the air gap size, on the order of surface roughness, is difficult to measure. Therefore, we employ a lumped nonlinear inductor model with an effective initial relative permeability μ_{eff}, which is a function of both the air gap permeability and core material permeability. The nonlinear inductor model supports a flux description that can be approximated as

$$\Lambda(t) = B_{\text{SAT}} A_{\text{CORE}} N \frac{2}{\pi} \arctan\left(\frac{N}{\beta} i_{\mu}(t)\right) \tag{1}$$

where B_{SAT} is the saturation flux density of the core material, A_{CORE} is the cross-sectional area of the core, N is the number of secondary turns, and $i_{\mu}(t)$ is the current through the magnetizing inductance [2]. β relates the mean magnetic flux path length l_{FLUX} and μ_{eff} and is defined as

$$\beta = l_{\text{FLUX}} \frac{2B_{\text{SAT}}}{\pi \mu_{\text{eff}} \mu_0}. \tag{2}$$

The effective initial relative permeability can be reliably estimated by measuring the magnetizing inductance L_{μ} of the clamped energy harvester using an impedance analyzer and solving the following equation for μ_{eff}:

$$L_{\mu} = \frac{\mu_{\text{eff}} \mu_0 N^2 A_{\text{CORE}}}{l_{\text{FLUX}}}. \tag{3}$$

An unfortunate consequence of both the core cutting process and the introduction of surface roughness air gaps when clamping the core back together is a significant decrease in μ_{eff} of the combined split core flux path [16]. A high-permeability core is very desirable for CT MEHs because the magnetizing inductance of the core is directly proportional to its permeability [3]. A larger magnetizing inductance yields both greater shunt impedance and allows the core to develop a wider range of voltage levels, such that the core can act as a more ideal current source.

A linear approximation for the effective initial relative permeability of a core with an air gap [17], is given by

$$\mu_{\text{eff}} = \frac{\mu_{\text{core}}}{1 + \frac{l_{\text{gap}}}{l_{\text{FLUX}}} \times \mu_{\text{core}}}. \tag{4}$$

Given a relatively high-permeability $\mu_{\text{core}} = 100000$ core with mean magnetic path length of 100 mm, we can see that even a small gap length of 1 μm results in a 50% decrease in effective initial relative permeability.

The flux description given in (1) can be implemented in SPICE and accurately describes harvester behavior in the unsaturated and saturated regimes for both the high-permeability ungapped cores referenced in previous work and in the relatively low-effective permeability split cores explored in this work. These claims are validated in Section III of this report. Circuit modeling in SPICE is an excellent way of predicting core behavior, but provides little insight and design intuition for the split core energy harvester designer. The significant contribution of this work is generalizing the analytical modeling approach from [2] to apply to any CT MEH, regardless of relative permeability or primary current excitation level. The simplified analytical formulas presented in the following are the starting point from which the CT MEH designer can begin a design and develop an intuition for core behavior. Then, circuit modeling can be used to refine a design.

B. Analytical Designer's Tools

Our goal in this section is to introduce analysis and discussion that provides both intuition for MEH behavior and also simplified expressions to quantify harvester behavior in order to closely predict general MEH performance. A rather surprising and unintuitive feature of magnetic energy harvesters is the phenomenon that maximum power harvest occurs when the core is subject to some level of saturation [2]. Many existing MEH works aim to avoid saturation [9], [12], and [18]. To optimize magnetic energy harvester capabilities, saturation is not something to be avoided altogether, but rather understood, modeled, and controlled.

In a practical application for a magnetic energy harvester, the core voltage will be rectified and provide power either to the dc supply rail of an MCU or sensor node or the input to a dc–dc converter stage. In either case, the load attached to the core during a half cycle of primary current can be modeled as a constant dc voltage V_{LOAD}. For this analysis, we assume a passive rectification scheme as it describes the uncontrolled saturating behavior of the harvester core. Assuming the harvester core can sustain a voltage greater than or equal to the dc load voltage, the average power harvest is

$$P_{\text{LOAD}} = \frac{2}{T}\int_{t_{\text{OPEN}}}^{t_{\text{CLOSE}}} i_{\text{LOAD}}(t)\cdot V_{\text{LOAD}}\,\mathrm{d}t = \frac{2}{T}\int_{t_{\text{OPEN}}}^{t_{\text{CLOSE}}} \left[\frac{I_P}{N}\sin(\omega t) - i_\mu(t)\right]\cdot V_{\text{LOAD}}\,\mathrm{d}t \quad (5)$$

where T is the period of the input current, t_{CLOSE} refers to the time during the half cycle at which power transfer to the load ceases, and t_{OPEN} refers to the time at which power transfer to the load begins each half cycle. Thus, t_{OPEN} and t_{CLOSE} define the "transfer window," a term used in the literature to describe the portion of a half cycle of primary current during which the core is relatively unsaturated, transferring power to the load [2]. While saturation is formally described by the magnetic flux density change with respect to the applied magnetic field, for the purposes of CT MEH design, we will formally define the saturation boundary based on the length of the transfer window. If the transfer window is a full $T/2$ long, then the core is "unsaturated". Otherwise, if $t_{\text{CLOSE}} - t_{\text{OPEN}} < T/2$, then the core is "saturated" to some degree. Adopting this definition of saturation is particularly useful in the CT MEH context. This definition is clear and measurable. When the core does not saturate whatsoever during the a half cycle of input current, $t_{\text{OPEN}} \approx 0$ and $t_{\text{CLOSE}} \approx T/2$ with respect to the primary current. More precisely, t_{OPEN} precedes the zero-crossing of the primary current, and consequently the transfer window closes earlier than $T/2$ as well. Generally, the core will saturate and should be allowed to saturate, or operate on the verge of saturation, if we are aiming to extract maximum power from the energy harvester. In this case, the transfer window is shortened due to core saturation, at which point the core magnetizing inductance begins to act more as a short circuit, shunting current away from the load. Under saturation, t_{OPEN} is what we will refer to as the "restoration time" of the core magnetizing inductance.

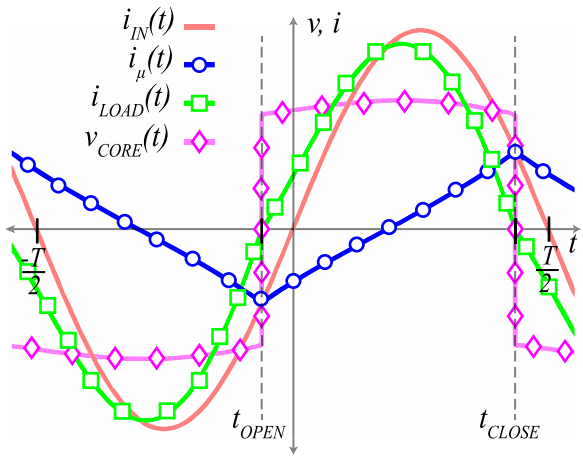

Fig. 4. Transfer window in the unsaturated case.

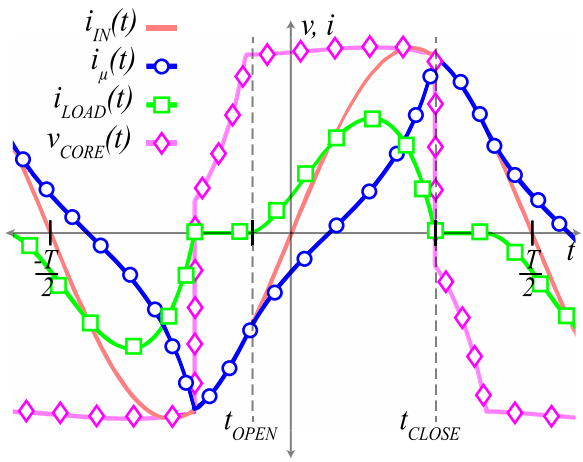

Fig. 5. Transfer window in a general saturated case.

This restoration time precedes the zero-crossing of the primary current and can be visualized as the position on a $B-H$ curve at which the core operating point has re-entered a linear operating regime. During this linear operating regime, the magnetizing inductance acts as a relatively large shunt impedance compared to the low impedance the core exhibits when saturated to some degree. t_{CLOSE} then describes the instance at which the core is saturated, which is the time when the core is saturated enough such that the core begins to carry all of the input current $i_{\text{IN}}(t)$, as shown in Fig. 3. This is also the point in time at which the core voltage drops rapidly through 0 V. Figs. 4 and 5 serve to accompany this defining of t_{OPEN} and t_{CLOSE} with respect to the input current waveform in both the unsaturated and saturated cases, respectively.

The real importance of t_{OPEN} and t_{CLOSE} manifests itself in the saturated operating regime of an MEH. Consider the case shown in Fig. 5 where we will define a time $t = 0$ at the origin, such that the negative half cycle of the shown period of the sinusoidal primary current has occurred prior to $t = 0$ and the positive half cycle of the primary current occurs after $t = 0$. As shown in Fig. 5, we will assume that the core has experienced some degree of saturation, which is key for assuming the core is

being operated at its maximum power harvest capabilities. The effect of t_{CLOSE} on power harvest is somewhat easily understood. When the core saturates prior to the next zero-crossing of the primary current at $t = T/2$, the saturated magnetizing inductance shunts current away from the load until the core eventually exits saturation at the opening of the next transfer window. An understanding of the restoration time and why it precedes the input current zero-crossing is more complicated. In the negative half cycle, as shown in Fig. 5, the core has been in saturation for some time until it reaches t_{OPEN}. During that saturation period prior to t_{OPEN}, the core magnetizing inductance carries nearly all of the input current. Right when the magnetizing inductance is "restored" to its linear operating regime at t_{OPEN}, it reassumes a large shunt impedance, but also behaves intuitively as one would expect an inductor to, restricting abrupt changes in current flow. The magnetizing current does not ramp down as quickly as the input current. By Kirchhoff's Current Law (KCL), the difference in the input current and magnetizing current must flow into the load. This current difference causes the transfer window to open at $t = t_{\text{OPEN}}$ prior to the input current zero-crossing, resulting in positive i_{LOAD} for a time period $t_{\text{OPEN}} \leq t < 0$ during which the input current is negative. The split core energy harvester designer must not only conceptually understand these constraints on the transfer window due to saturation and restoration effects, but also precisely quantify t_{OPEN} and t_{CLOSE} in order to predict average harvester power output. In order to quantify these transfer window bounds, we first assume that the core is experiencing some degree of saturation, then if our calculations under that assumption yield a transfer window equal to a full-half cycle of input current ($t_{\text{CLOSE}} - t_{\text{OPEN}} = T/2$), we modify our assumptions to account for no saturation, and recalculate the transfer window bounds properly.

We can relate the voltage across the magnetizing inductance at $t = t_{\text{OPEN}}$ to the derivative of the flux density through the core as

$$v_{\text{CORE}}(t) = \frac{\partial \Lambda(t)}{\partial t} = A_{\text{CORE}} N \frac{\partial B(t)}{\partial t}. \tag{6}$$

We will also now express $B(t)$ explicitly as

$$B(t) = B_{\text{SAT}} \frac{2}{\pi} \arctan\left(\frac{N}{\beta} i_\mu(t)\right) = \gamma \arctan(\zeta\, i_\mu(t)) \tag{7}$$

where we have defined $\gamma = B_{\text{SAT}}\, 2/\pi$ and $\zeta = N/\beta$ to condense the number of terms in the following analysis. Differentiating $B(t)$ with respect to t at $t = t_{\text{OPEN}}$ yields

$$\frac{\partial B(t_{\text{OPEN}})}{\partial t} = \frac{\gamma \zeta \omega I_P \cos(\omega t_{\text{OPEN}})}{N(1 + \zeta^2 (\frac{I_P}{N} \sin(\omega t_{\text{OPEN}}))^2} \tag{8}$$

where we have made key assumptions that at $t = t_{\text{OPEN}}$, the magnetizing current $i_\mu(t)$ is equal to the input current $(I_P/N)\sin(\omega t)$, and the magnetizing current derivative is the same as that of the input current, which is evident in Fig. 5. It is essential to note that these assumptions are only true in the presence of saturation. Substituting (8) into (6) gives

$$V_{\text{LOAD}} = A_{\text{CORE}} \left[\frac{\gamma \zeta \omega I_P \cos(\omega t_{\text{OPEN}})}{1 + \zeta^2 (\frac{I_P}{N} \sin(\omega t_{\text{OPEN}}))^2} \right] \tag{9}$$

where we can now solve (9) for t_{OPEN} as

$$t_{\text{OPEN}} = -\frac{1}{\omega} \arccos\left(\frac{X - Y}{Z}\right) \tag{10}$$

where

$$X = \sqrt{A_{\text{CORE}}^2 \gamma^2 N^4 \omega^2 + 4 N^2 V_{\text{LOAD}}^2 + 4\zeta^2 I_P^2 V_{\text{LOAD}}^2}$$
$$Y = A_{\text{CORE}} \gamma N^2 \omega$$
$$Z = 2\zeta I_P V_{\text{LOAD}}.$$

We can then equate the change in core flux density to the time integral of the core voltage over a transfer window as

$$\Delta B A_{\text{CORE}} N = \int_{t_{\text{OPEN}}}^{t_{\text{CLOSE}}} V_{\text{LOAD}} \mathrm{d}t \tag{11}$$

where ΔB is defined as

$$\Delta B = B(t = t_{\text{CLOSE}}) - B(t = t_{\text{OPEN}}). \tag{12}$$

$B(t = t_{\text{OPEN}})$ can be solved for using (7), since the magnetizing current is equal to the input current at time $t = t_{\text{OPEN}}$. $B(t = t_{\text{CLOSE}})$ can also be described in terms of the input current, since the magnetizing current is also equal to the input current at time $t = t_{\text{CLOSE}}$. Therefore, (11) can be rewritten as

$$\left[\gamma \arctan\left(\zeta \frac{I_P}{N} \sin(\omega t_{\text{CLOSE}})\right) - B(t = t_{\text{OPEN}})\right] A_{\text{CORE}} N = \int_{t_{\text{OPEN}}}^{t_{\text{CLOSE}}} V_{\text{LOAD}}\, \mathrm{d}t. \tag{13}$$

While the only unknown in (13) is t_{CLOSE}, solving (13) is computationally intensive, since (13) takes the form of a transcendental equation with no closed-form solution. A useful approximation for $B(t = t_{\text{CLOSE}})$ can be made in order to simplify (11) in a way that allows us to obtain a closed-form solution for t_{CLOSE}. Since the magnetizing current is upper bounded by the maximum input current, we can conclude that $B(t = t_{\text{CLOSE}})_{\text{MAX}}$ is

$$B(t = t_{\text{CLOSE}})_{\text{MAX}} = \gamma \arctan\left(\zeta \frac{I_P}{N}\right). \tag{14}$$

Similarly, the magnitude of $B(t = t_{\text{CLOSE}})$ is lower bounded by $B(t = t_{\text{OPEN}})$, which is exactly the flux density magnitude at which the core exits the nonlinear saturation regime of its $B - H$ curve. Thus,

$$B(t = t_{\text{CLOSE}})_{\text{MIN}} = -B(t = t_{\text{OPEN}}). \tag{15}$$

We then approximate $B(t = t_{\text{CLOSE}})$ as the average of its upper and lower bounds as

$$B(t = t_{\text{CLOSE}}) \approx \frac{B(t = t_{\text{CLOSE}})_{\text{MAX}} + B(t = t_{\text{CLOSE}})_{\text{MIN}}}{2}. \tag{16}$$

The abovementioned approximation is simply one of many approximations we could have made in order to move forward with the analysis to obtain a closed-form solution for t_{CLOSE}. The

choice of other, potentially better, approximations will be discussed as follows. With our approximation for $B(t = t_{\text{CLOSE}})$, (12) simplifies to

$$\Delta B = \frac{\gamma \arctan\left(\zeta \frac{I_P}{N}\right) - 3B(t = t_{\text{OPEN}})}{2}, \tag{17}$$

which can be combined with (11) to solve for t_{CLOSE} as

$$t_{\text{CLOSE}} = \min\left[\frac{\Delta B A_{\text{CORE}} N}{V_{\text{LOAD}}} + t_{\text{OPEN}}, \frac{T}{2} + t_{\text{OPEN}}\right]. \tag{18}$$

If (18) returns $t_{\text{CLOSE}} = T/2 + t_{\text{OPEN}}$, the transfer window is a full-half cycle of input current long, and we know that the core is not experiencing saturation. The fact that the transfer window is a full-half cycle long contradicts our abovementioned assumptions about the derivative of the magnetizing current being equal to the derivative of the input current and the value of $B(t = t_{\text{CLOSE}})$, which only held under saturation conditions. We recalculate t_{OPEN} and t_{CLOSE} by using the same flux equality method, but under different assumptions as follows. In nonsaturation, we can assume that

$$t_{\text{CLOSE}} - t_{\text{OPEN}} = \frac{T}{2}$$
$$B(t = t_{\text{CLOSE}}) = -B(t = t_{\text{OPEN}}).$$

The transfer window assumption is valid, because the transfer window must be a full $T/2$ long if the core does not saturate, and the flux density assumption is valid because in nonsaturation, as stated above, if the transfer window opens early (with respect to $t = 0$) by a time t_{OPEN}, then the window closes early by the same amount of time (with respect to $T/2$) at t_{CLOSE}. This means that the magnetizing current with respect to the sinusoidal input current is equal in magnitude and opposite in time at times t_{OPEN} and t_{CLOSE}, and therefore the core flux densities at those times must also be equal in magnitude and opposite in sign. Under these new assumptions

$$\Delta B = -2B(t = t_{\text{OPEN}}) \tag{19}$$

and the flux equality of (11) can be rewritten as

$$-2B(t = t_{\text{OPEN}}) A_{\text{CORE}} N = V_{\text{LOAD}} \frac{T}{2}. \tag{20}$$

Substituting the definition of $B(t)$ given in (7), we obtain the following closed-form solution for t_{OPEN}:

$$t_{\text{OPEN}} = -\frac{1}{\omega} \arcsin\left(\frac{N}{I_P \zeta} \tan\left(\frac{T}{4} \frac{V_{\text{LOAD}}}{A_{\text{CORE}} \gamma N}\right)\right). \tag{21}$$

Since we know this is a nonsaturation case, we simply add $T/2$ to t_{OPEN} to obtain our value for t_{CLOSE}.

The abovementioned equations provide analytical expressions from which the magnetic energy harvester designer can quantitatively define the transfer window over a half cycle of primary current. Defining the bounds of the transfer window quantitatively is imperative for predicting core power harvest capabilities over a wide range of load voltages using (5).

The remaining unknown in (5) for solving average power harvest is $i_\mu(t)$. Returning to (6) and carrying out the time differentiation on $B(t)$, we obtain the following first-order nonlinear differential equation in terms of $i_\mu(t)$:

$$V_{\text{LOAD}} = \frac{\gamma A_{\text{CORE}} N \zeta}{1 + \zeta^2 i_\mu(t)^2} \left(\frac{\partial i_\mu(t)}{\partial t}\right). \tag{22}$$

Applying the initial condition $i_\mu(t_{\text{OPEN}}) = (I_P/N) \sin(\omega t_{\text{OPEN}})$ gives the following solution for $i_\mu(t)$:

$$i_\mu(t) = \frac{1}{\zeta} \tan\left[\frac{V_{\text{LOAD}}(t = t_{\text{OPEN}})}{\gamma A_{\text{CORE}} N} + \arctan\left(\zeta \frac{I_P}{N} \sin(\omega t_{\text{OPEN}})\right)\right] \tag{23}$$

which can be integrated over the transfer window to solve for average power harvest. Equation (5) can be equivalently rewritten as

$$P_{\text{LOAD}} = \frac{2}{T} V_{\text{LOAD}} \left[\int_{t_{\text{OPEN}}}^{t_{\text{CLOSE}}} \frac{I_P}{N} \sin(\omega t)\, \mathrm{d}t - \int_{t_{\text{OPEN}}}^{t_{\text{CLOSE}}} i_\mu(t)\, \mathrm{d}t\right] \tag{24}$$

where the average power harvest is now expressed in the form of all known quantities. A simple numerical analysis of (24) over a wide V_{LOAD} sweep can quickly provide an MEH designer with an optimal V_{LOAD} for a given core design and primary current or similarly with an optimal N turns for a given core, primary current, and target V_{LOAD}.

We now consider the agreement between the generalized analysis proposed in this work and the existing specific analysis for a very high-permeability nanocrystalline core [2]. The agreement can be intuitively understood by considering the behavior of the arctangent function, which we use to describe the flux density of the harvester, over different domain ranges. Consider the function

$$f(x) = \arctan(Ax) \tag{25}$$

where A is a positive real constant. We can fix $A = 1$ and plot $f(x)$ over two different domain ranges of x: 1) [−5,5]; and 2) [−1,1], as shown in Fig. 6. Similarly, we can fix a domain range of x between −1 and 1, and plot $f(x)$ for multiple values of A, as shown in the shaded region of Fig. 6. The arctangent function assumes a different shape over different x domains and different A values. These illustrations serve as visual distinctions between the general model proposed in this work and that presented in [2]. In this discussion, A is proportional to μ_{eff} and x is

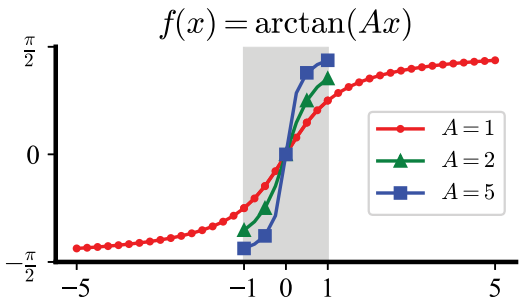

Fig. 6. Domain x and coefficient A of the arctangent function describe varying saturation behavior.

proportional to $i_\mu(t)$, which will increase proportionally with I_P. In our MEH design context, we consider typical primary current ranges for industrial electromechanical machinery of 1–100 A (our "x" domains). Imagine a design comparison in which two MEH cores of the same dimensions and material: 1) one split core; and 2) one ungapped, have the same B_{SAT}. The split core will have a significantly lower μ_{eff} than the ungapped core. We can use Fig. 6 to understand how primary current excitations I_P and μ_{eff} affect the behavior of a saturating MEH. The case of the extremely high-permeability core corresponds to the large A case in Fig. 6. The arctangent curve traverses essentially its full range $[-\pi/2, \pi/2]$, and does so in a relatively small percentage of the total shown x domain. An extremely high-permeability nanocrystalline core with initial relative permeability in the hundreds of thousands would yield a similar "large A" arctangent shape for its flux traversal. Through this reasoning, it becomes apparent why Moon and Leeb [2] were able to conclude early in their analysis that $\Delta B = 2B_{\text{SAT}}$ over a half cycle.

Generally, a magnetic energy harvester core will not have an extremely large μ_{eff} relative to the primary current, as is the case for easily installed split cores explored in this work. When experimentally characterizing high-permeability nanocrystalline split cores, which have μ_{eff} on the order of 10 000, the $\Delta B = 2B_{\text{SAT}}$ assumption does not hold in the 1–10-A rms primary current range. Power output capabilities will be significantly overpredicted in such cases, since the core is realistically only swinging some fraction of $2B_{\text{SAT}}$ every half cycle in this specific example. This is represented by the shaded portion of the $A = 1$ case shown in Fig. 6. Given the same split cores under significantly higher primary current conditions, say 50-A rms, one can expect that the $\Delta B = 2B_{\text{SAT}}$ approximation is more reasonable. As illustrated by the $\arctan(Ax)$ exercise, even a "low" permeability core will exhibit a $2B_{\text{SAT}}$ flux density swing if subject to a large enough primary current. Similarly, any "high" permeability core could show a significantly smaller ΔB if subject to low enough primary current conditions. The estimated flux swing per half cycle of input current is generally a function of the effective core permeability, system current levels, and the flux density describing function. While we have employed the arctangent function in this work, it is reasonable to assume that there may be a more accurate flux density describing function for a different harvester core. Regardless of the chosen flux density function, arctangent, piecewise, or another, the same intuitive argument applies. The $\Delta B = 2B_{\text{SAT}}$ assumption, which is prevalent in the saturating energy harvester literature [2], [11], does not generally hold. The MEH designer must consider the core material properties μ_{eff} and B_{SAT}, input current excitation levels, and $B - H$ describing curve in making assumptions about the flux density swing in the abovementioned analysis.

For example, in the abovementioned derivation, we have chosen to approximate $B(t = t_{\text{CLOSE}})$ in the presence of saturation as the average of its upper and lower bounds in order to obtain a closed-form solution for t_{CLOSE}. This is just one example of many possible approximations an MEH designer can choose. We chose the average approximation as a general, somewhat neutral example, but the abovementioned analysis method is valid, given other approximations for $B(t = t_{\text{CLOSE}})$, and the MEH designer should choose an approximation given their knowledge of the core material choice, dimensions, turns, and primary current levels in the application space.

Another differentiation between our expression for average power harvest given in (24) is that our integral includes $i_\mu(t)$ term. The results, however, do agree. The magnetizing inductance impedance is directly proportional to the magnetizing inductance L_μ, which in turn is directly proportional to μ_{eff}. Therefore, given an extremely high μ_{eff} core, one can reasonably conclude that $i_\mu = 0$ over the transfer window, since the magnetizing inductance is relatively unsaturated during this time and the magnetizing inductance and load branch act as current divider. This approximation is not valid in the case of a relatively low μ_{eff} split core.

This section has proposed generalized analytical methods for defining the transfer window of an MEH, which is essential for modeling and maximizing power harvest. Using these methods, the MEH designer both gains an intuition for and numerically defines power harvest capabilities of a design under different load conditions. These models can also be employed to help solve for optimal harvester design parameters given load and core size constraints. For example, given an installation site for the harvester with a specific primary current range and volume constraint for the harvester node, a designer can sweep for optimal N and/or optimal V_{LOAD} levels, such that the core operates at or around its maximum power point over the entire installation site primary current range. Furthermore, a designer can exploit the relative simplicity of the analysis compared to numerical solvers, such as SPICE, in order to allow a processing unit to calculate and perhaps maximize its own harvester's power harvest in real-time.

III. Core Performance and Model Validation

This section explores the output power capabilities of two high-permeability nanocrystalline split cores and one extremely high-permeability ungapped nanocrystalline core. This section validates both the circuit analytical models presented in Section II for an MEH practical use case, in which the harvester core is connected to a dc voltage load through a full-bridge passive rectifier. Passive rectifier diode forward voltage drops were included in the analytical and circuit modeling in order to most accurately predict core power harvest. The electric circuit model shown in Fig. 3 was implemented in LTSpice, where the magnetizing inductance was modeled via the nonlinear flux description given in (1). For SPICE implementation of the circuit model in Fig. 3, the core loss resistor can be estimated with methods, as mentioned above [2], or can be ignored, as we have done in this work because of the extremely low losses of our nanocrystalline cores. The rms primary current I_P is a given or known parameter. L_{LEAK} can be measured using an open/short circuit measurement technique with an impedance analyzer as commonly used for determining magnetizing and leakage inductances of all sorts of electrical transformers. Leakage inductance is often negligible in the case of these very high-permeability core materials. R_{WIRE} can be measured using

TABLE I
MODEL PARAMETERS

Core	A_{CORE} [mm^2]	l_{FLUX} [mm]	B_{SAT} [T]	L_μ [H]	μ_{eff}	$R_{CORE}[\Omega]$	L_{LEAK} [H]	$R_{WIRE}[\Omega]$
$N = 300$ Split	75	72.7	1.0	1.04	8914	$\approx \infty$	≈ 0	4.8
$N = 600$ Split	75	72.7	1.0	4.70	10071	$\approx \infty$	≈ 0	9.6
$N = 100$	40	78.5	1.24	0.927	144770	$\approx \infty$	≈ 0	0.100

a Kelvin measurement technique with an impedance analyzer or analytically estimated based on wire gauge and material.

The dimensions, saturation flux densities, magnetizing inductances, and initial effective relative permeabilities of three cores of interest are listed in Table I. The split cores used are toroidal nanocrystalline cut-cores manufactured upon request by CoilCore and have 300 and 600 turns, respectively. Each of the split cores evaluated in this work has an outer diameter of 28.5 mm, an inner diameter of 18.5 mm, and a height of 15 mm, where each core weighs approximately 33 g, maintaining a lightweight unit that could feasibly be noninvasively installed about a current-carrying power line. The 100-turn core is an ungapped core and is a Vacuumschmelze W423 toroidal core of magnetic material Vitroperm 500 F. Magnetizing inductances were measured at 65 Hz using an impedance analyzer and the μ_{eff} of each core was determined using (3). Such core dimensions are reasonable sizes for a self-powered sensing unit that would fit into a typical National Electrical Manufacturers Association (NEMA) enclosure for an industrial electric machine. Each of the nanocrystalline split cores, which have a core material permeability on the order of 100 000 after the cutting process according to the manufacturer, exhibits a μ_{eff} of approximately 9000, implying surface roughness air gaps of about 2.5 μm at each of the mating surfaces. The implied surface roughness is consistent with typical surface roughness of core mating surfaces after common laser and wire cutting techniques [10]. It is important to note that split core μ_{eff}, even for cores of the same material, will vary dramatically with gap length, as described in (4). The gap length must be well-controlled in order to ensure repeatability of core power harvest performance. In this work, gap length was controlled throughout experiments by tightly clamping the core semitoroids together with good alignment and adjusting the clamping force on the semitoroids to ensure that a given core's magnetizing inductance remained consistent during experiments. While material permeability will vary slightly among split cores of the same material, and gap length is the dominating factor in determining overall μ_{eff} of the core flux path. Leakage inductance was measured to be approximately 1% or less of the magnetizing inductance for each of the cores of interest and is thus ignored in the modeling.

The cores were connected to a full-bridge passive Schottky diode rectifier (KMB22STR) and dc voltage load. The dc voltage load was swept over a wide operating range, subjecting the core to deeper saturation at larger voltage loads. An annotated picture of the experimental setup is shown in Fig. 7. Fig. 8 through Fig. 11 compare the predicted output powers based on the analytical modeling and SPICE modeling to experimental results over the dc voltage load sweep. The edge of saturation, as defined by the abovementioned transfer window length, is determined by our analytical model and marked in a golden dotted vertical

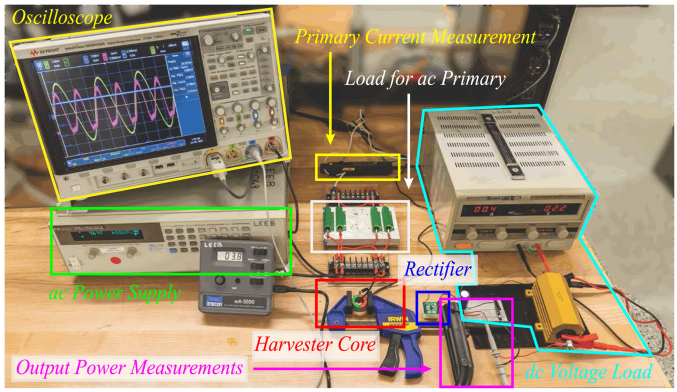

Fig. 7. Lab bench experimental setup.

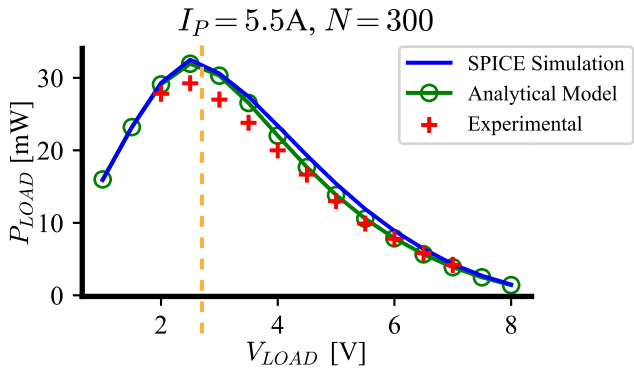

Fig. 8. N = 300 split core at I_P = 5.5-A rms.

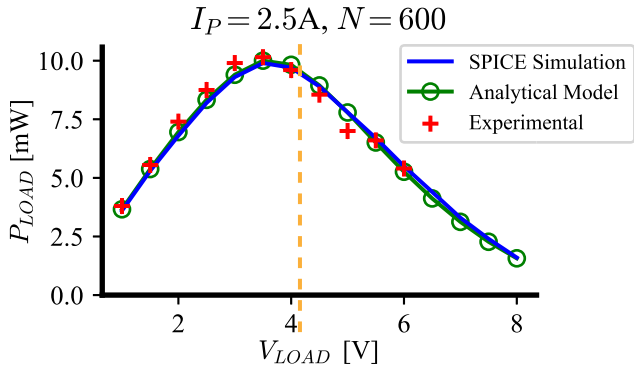

Fig. 9. N = 600 split core at I_P = 2.5-A rms.

line in each figure. More specifically, the left-hand side of the dotted line, the core is "unsaturated", providing load current for a full-half cycle of input current. On the right-hand side of the dotted line, the core is "saturated", providing load current for less than a half cycle of input current. The V_{LOAD} ranges differ between experiments. This is because each core magnetizing inductance L_μ is capable of sustaining a finite V_{LOAD} range

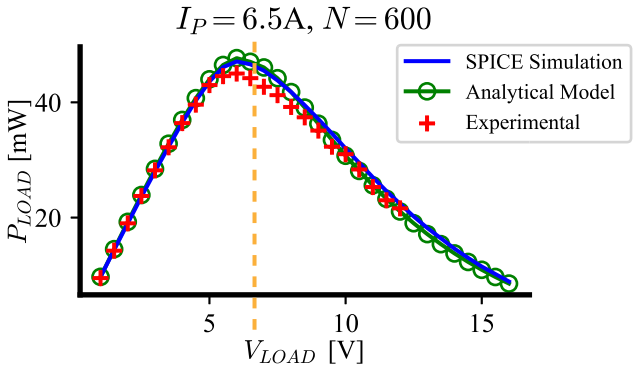

Fig. 10. N = 600 split core at $I_P = 6.5$-A rms.

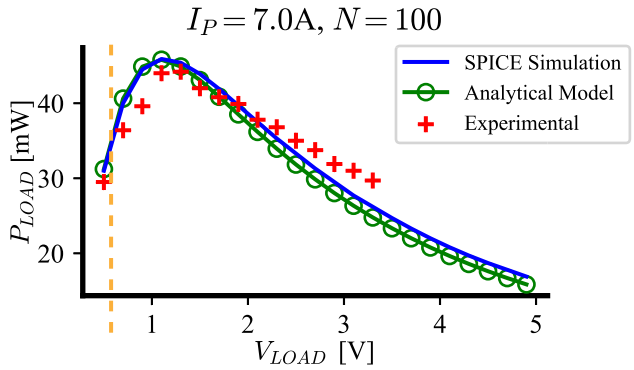

Fig. 11. Ungapped core at $I_P = 7.0$-A rms.

based on its number of turns N and primary current excitation level. More precisely, the peak voltage any given inductance can sustain is

$$V_{L,\mathrm{PK}} = \omega N A_{\mathrm{CORE}} B_{\mathrm{PK}} = \omega N^2 \frac{A_{\mathrm{CORE}}}{l_{\mathrm{FLUX}}} \mu_{\mathrm{eff}} i_{L,\mathrm{PK}} \tag{26}$$

where B_{PK} and $i_{L,\mathrm{PK}}$ are the peak flux density and peak current through the inductance, respectively. The sustainable voltage load range of each core magnetizing inductance, therefore, will vary depending on core size, turns N, permeability, and system current levels. The cores were evaluated at multiple rms primary current levels, further validating the comprehensiveness of our modeling approach.

Both the analytical and SPICE modelings are fairly sensitive to small variations in μ_{eff} and B_{SAT}. As described in (4), small changes in gap length have drastic impacts on μ_{eff}. For our split cores under test in this work variations of merely 0.1 μm in gap length would cause approximately 5% variations in μ_{eff} from the measured values recorded in Table I. According to core manufacturer specifications, the nanocrystalline split cores used in our experiments have $\mu_{\mathrm{core}} \approx 100000$ after cutting. Combining this information with (4) and our measured μ_{eff} values given in Table I implies that the gap length due to surface roughness is approximately 3–4 μm at each toroid face (for a total $l_{\mathrm{gap}} \approx 7\mu$m). This surface roughness gap length is consistent with known residual effects of common core cutting techniques [10]. Variations of 0.1 μm are less than 10% of this total gap length, and it is quite reasonable to assume such variations occur during experimentation despite core clamping efforts. For demonstrations' sake, a 5% increase in μ_{eff} and a 5% decrease in μ_{eff} from the μ_{eff} value listed in Table I was applied to the modeling for the data included in Figs. 9 and 10, respectively.

IV. Conclusion

This article proposed and validated a generalized analytical model for predicting power harvest capabilities of saturating split core CT MEHs. An unintuitive feature of MEHs was highlighted; the harvester exhibited maximum power harvest at the edge of, and even into, the saturated regime of the core, which motivates the necessity for modeling power harvest into saturation. Split core CT MEHs behave as effectively lower permeability ungapped cores, with the significant convenience of noninvasive installation about a power line. Existing circuit model techniques proposed in [2] were validated for nanocrystalline split cores, and a generalized analytical model was proposed, which applies to any saturating toroidal CT MEH, including the relatively low μ_{eff} split cores experimented in this work. Intuition regarding CT MEHs was discussed. Despite the well-documented poor machinability of nanocrystalline cores, output power levels upwards of 45 mW were demonstrated on a 5.45 cm^3 nanocrystalline split core at primary current levels less than 7-A rms, proving the viability of nanocrystalline split cores as 60-Hz CT MEHs for powering compact sensing and other CBM units. Future work will aim to explore power harvest enhancement strategies, such as the addition of a resonant capacitance in order to increase harvester load voltage capabilities [21] or shaping the flux across the core magnetizing inductance with passive components or active switch control [22].

References

[1] O. B. Akan, O. Cetinkaya, C. Koca, and M. Ozger, "Internet of hybrid energy harvesting things," *IEEE Internet Things J.*, vol. 5, no. 2, pp. 736–746, Apr. 2018, doi: 10.1109/JIOT.2017.2742663.

[2] J. Moon and S. B. Leeb, "Analysis model for magnetic energy harvesters," *IEEE Trans. Power Electron.*, vol. 30, no. 8, pp. 4302–4311, Aug. 2015, doi: 10.1109/TPEL.2014.2357448.

[3] J. Moon, J. Donnal, J. Paris, and S. B. Leeb, "VAMPIRE: A magnetically self-powered sensor node capable of wireless transmission," in *Proc. IEEE 28th Annu. Appl. Power Electron. Conf. Expo.*, 2013, pp. 3151–3159.

[4] S. Yuan, Y. Huang, J. Zhou, Q. Xu, C. Song, and P. Thompson, "Magnetic field energy harvesting under overhead power lines," *IEEE Trans. Power Electron.*, vol. 30, no. 11, pp. 6191–6202, Nov. 2015, doi: 10.1109/TPEL.2015.2436702.

[5] S. Yuan, Y. Huang, J. Zhou, Q. Xu, C. Song, and G. Yuan, "A high-efficiency helical core for magnetic field energy harvesting," *IEEE Trans. Power Electron.*, vol. 32, no. 7, pp. 5365–5376, Jul. 2017, doi: 10.1109/TPEL.2016.2610323.

[6] W. Jiang, J. Lu, F. Li, S. Hashimoto, and Z. Lin, "A non-intrusive magnetic energy scavanger for renewable power generation state monitoring," in *Proc. IEEE Int. Conf. Renewable Energy Res. Appl.*, 2016, pp. 562–566.

[7] M. J. Vos, "A magnetic core permeance model for inductive power harvesting," *IEEE Trans. Power Electron.*, vol. 35, no. 4, pp. 3627–3635, Apr. 2020, doi: 10.1109/TPEL.2019.2933133.

[8] R. H. Bhuiyan, R. A. Dougal, and M. Ali, "A miniature energy harvesting device for wireless sensors in electric power system," *IEEE Sensors J.*, vol. 10, no. 7, pp. 1249–1258, Jul. 2010, doi: 10.1109/JSEN.2010.2040173.

[9] S. Paul, S. Bashir, and J. Chang, "Design of a novel electromagnetic energy harvester with dual core for deicing device of transmission lines," *IEEE Trans. Magn.*, vol. 55, no. 2, Feb. 2019, Art no. 8000104, doi: 10.1109/TMAG.2018.2873012.

[10] W. Zhou, Z. Liu, Q. Huang, Y. Jiang, and Z. Cong, "Design of magnetic cores for current transformer energy harvesting devices," in *Proc. IEEE PES Asia–Pacific Power Energy Eng. Conf.*, 2019, pp. 1–5.
[11] B. Park et al., "The magnetic energy harvester with improved power density using saturable magnetizing inductance model for maintenance applications near high voltage power line," *IEEE Access*, vol. 9, pp. 82661–82674, 2021, doi: 10.1109/ACCESS.2021.3085989.
[12] Y. Zhuang et al., "Improving current transformer-based energy extraction from AC power lines by manipulating magnetic field," *IEEE Trans. Ind. Electron.*, vol. 67, no. 11, pp. 9471–9479, Nov. 2020, doi: 10.1109/TIE.2019.2952795.
[13] J. G. Kassakian, F. M.Schlecht, and G. C. Verghese, *Principles of Power Electronics*, 1st ed.Boston, MA, USA: Addison-Wesley, 1991.
[14] T. Kauder and K. Hameyer, "Iron loss comparison of standard SiFe and nanocrystalline materials for power transformers in a dual active bridge converter," in *Proc. IEEE 18th Eur. Conf. Power Electron. Appl.*, 2016, pp. 1–10.
[15] T. Kauder and K. Hameyer, "Performance factor comparison of nanocrystalline, amorphous, and crystalline soft magnetic materials for medium-frequency applications," *IEEE Trans. Magn.*, vol. 53, no. 11, pp. 1–4, Nov. 2017, doi: 10.1109/TMAG.2017.2702184.
[16] K. Draxler, J. Hlavaček, R. Prochazka, M. Knenicky, and R. Styblikova, "Clamp current transformers for noninvasive calibration of current transformers," in *Proc. IEEE Int. Instrum. Meas. Technol. Conf. Proc.*, 2016, pp. 1–6.
[17] C. W. T. McLyman, *Transformer and Inductor Design Handbook*, 3rd ed. New York, NY, USA: Marcel Dekker Inc., 2004.
[18] C. Tan, Y. Zhao, and Z. Tang, "Study on energy harvesting of open-close current transformer," in *Proc. Int. Conf. Sens., Meas. Data Analytics Era Artif. Intell.*, 2020, pp. 567–571.
[19] J. Moon and S. B. Leeb, "Enhancement on energy extraction from magnetic energy harvesters," in *Proc. IEEE Energy Convers. Congr. Expo.*, 2015, pp. 427–433.
[20] Y. Zhuang et al., "An improved energy harvesting system on power transmission lines," in *Proc. IEEE Wirel. Power Transfer Conf.*, 2017, pp. 1–3.
[21] Q. Sun, S. Patil, N.-X. Sun, and B. Lehman, "Inductive magnetic harvester with resonant capacitive rectifier based on synchronized switch harvesting technique," in *Proc. IEEE Energy Convers. Congr. Expo.*, 2013, pp. 4940–4947.
[22] J. Moon and S. B. Leeb, "Power electronic circuits for magnetic energy harvesters," *IEEE Trans. Power Electron.*, vol. 31, no. 1, pp. 270–279, Jan. 2016, doi: 10.1109/TPEL.2015.2401336.

Daniel Monagle (Graduate Student Member, IEEE) received the B.S. and S.M. degrees in electrical engineering and computer science, in 2020 and 2022, respectively, from the Massachusetts Institute of Technology, Cambridge, MA, USA, where he is currently working toward the Ph.D. degree in electrical engineering and computer science.

His research interests include energy harvesting, magnetics, low-power circuit design, and self-powered systems.

Eric Ponce received the B.S. degree in electrical science and engineering and M.Eng. degree in electrical engineering and computer science, in 2017 and 2019, respectively, from the Massachusetts Institute of Technology, Cambridge, MA, USA, where he is currently working toward the Ph.D. degree in electrical engineering and computer science.

Steven B. Leeb (Fellow, IEEE) received the doctoral degree in electrical engineering and computer science from the Massachusetts Institute of Technology (MIT), Cambridge, MA, USA, in 1993.

He was a Commissioned Officer with United States Air Force Reserves. Since 1993, he has been a Member of MIT Faculty, Department of Electrical Engineering and Computer Science. He also holds a joint appointment with the Department of Mechanical Engineering, MIT. He has authored or coauthored more than 200 publications and 20 U.S. Patents in the fields of electromechanics and power electronics.